Proceedings of the 17th World Congress
The International Federation of Automatic Control
Seoul, Korea, July 6-11, 2008

Two-Degree-of-Freedom Tracking Control of Piezoelectric Tube Scanners in Two-Dimensional Scanning Applications

J. Maess * **J. Becker** ** **L. Gaul** ** **F. Allgöwer** *

* *Institute for Systems Theory and Automatic Control, Universität Stuttgart, Pfaffenwaldring 9, 70550 Stuttgart, Germany (email: {maess,allgower}@ist.uni-stuttgart.de).*
** *Institute of Applied and Experimental Mechanics, Universität Stuttgart, Pfaffenwaldring 9, 70550 Stuttgart, Germany (email: {becker,gaul}@iam.uni-stuttgart.de).*

Abstract: The precision of the raster scan motion of piezoelectric tube scanners, e.g. in scanning probe microscopy, is degraded by structural vibrations excited by the driving voltage signals. In order to eliminate these vibrations, a model–based, flatness–based feedforward control scheme is proposed that tracks the tip of the piezoelectric tube along the desired scan trajectory in the lateral plane. This scheme is derived from a modal analysis of the tube scanner dynamics which is obtained by finite element (FE) discretization. In order to achieve robustness of the trajectory tracking performance with respect to model errors or unknown external disturbances, the feedforward control is supplemented by a feedback controller in a two–degree–of–freedom design which feeds back the measured displacements at the top of the scanner. The feedback additionally compensates for the coupling between the two scanning directions, e.g. due to tube eccentricity. The control performance is investigated in simulations where the sample mass attached to the top of the tube, which represents the most realistic model error, is varied. Various simulation results demonstrate the achieved improvements in tracking accuracy by the proposed control over conventional approaches.

Keywords: Feedforward control; Finite element analysis; Distributed parameter systems; Mechanical systems; Tracking applications.

1. INTRODUCTION

Piezoelectric tubes were used for nanopositioning and nanofabrication applications by Binning and Smith (1986) for the first time. They feature three–dimensional displacement with high resolution and are thus the predominant scanner design in scanning probe microscopy (Sun and Wolkow (2006)). However, the scan accuracy as well as the scan speed are limited due to the excitation of the low-frequency resonances of the piezoelectric tube by the driving voltages. Several approaches for vibration suppression have been investigated, including feedforward control (Li and Bechhoefer (2007)), feedback control (Schitter et al. (2004)), and piezoelectric shunt damping (Fleming and Moheimani (2006)).

The piezoelectric scanner depicted in Fig. 1 consists of a thin-walled cylindrical tube of radially polarized piezoceramic material and is mechanically clamped at the lower end. The inner surface of the tube is coated by a grounded electrode, and four evenly spaced quartered electrodes are deposited on the outer diameter representing the potential or actuator electrodes driven by external voltages. The driving voltages $+u_\mathrm{x}$ and $-u_\mathrm{x}$ of equal magnitude but opposite sign are applied to the corresponding pair of x^+– and x^-–electrodes centered above the x–axis in the twin-electrode excitation mode. Respectively, the voltages $+u_\mathrm{y}$ and $-u_\mathrm{y}$ are the inputs to the y–axis electrodes. Application of the driving voltages causes a bending motion of the tube along the directions of the potential differences, generating the displacements w_x and w_y at the free end of the tube.

To exploit the apriori knowledge of the two-dimensional raster scan motion in the lateral xy-plane, a feedforward control scheme for trajectory tracking is applied to the piezoscanner. Together with the feedback controller, the feedforward tracking leads to a two-degree-of-freedom control of the piezoscanner. The feedfoward approach developed by Becker and Meurer (2007) is based on a combination of modal analysis and differential flatness. Finite Element Analysis (FEA) is applied for the derivation of the underlying modal representation of the piezoscanner dynamics. To take advantage of the high accuracy and detailed geometrical modeling of the FEA, the model accounts for a sample mass attached to the top of the tube (see Fig. 1). Furthermore, the coupling effects between the motion in x- and y-direction (Tien et al. (2005)), stemming e.g. from tube eccentricity due to machining tolerances (El Rifai and Youcef-Toumi (2001)), are included in the FE-model for simulation in order to demonstrate the compensation performance of the feedback control.

2. FINITE-ELEMENT MODEL OF THE PIEZOELECTRIC TUBE SCANNER

Suitable models are needed for the proposed model–based control design. In (Carr (1988)), the modeling of piezoelectric tube scanners by FEA is restricted to static analysis. This static approach is extended by Sun and Wolkow (2006) to a tube

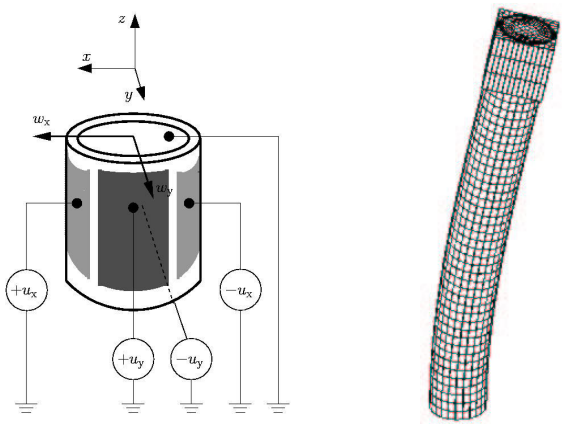

Fig. 1. Electrode circuitry for a piezotube in twin–electrode excitation mode and FE model of tube assembly.

assembly taking the sample holder into account. In (Maess et al. (2007)), a dynamic analysis of the piezoelectric tube is carried out and is generalized to the tube assembly in the following making use of finite–element (FE) discretization and a modal reduction approach.

The direct and indirect piezoelectric effects couple the structural and piezoelectric domains as described by the constitutive equations in stress–charge representation

$$T = c^{\mathrm{E}} S - eE$$
$$D = eS + \varepsilon^{\mathrm{S}} E,$$

where T denotes the mechanical stress matrix, S the mechanical strain matrix, E the electric field vector, D the electric charge vector per unit area, c^{e} the mechanical stiffness matrix at constant electric field, ε^{S} the permittivity matrix under constant strain, and e the piezoelectric matrix.

For the FE discretization, the mechanical and electrical fields as unknown quantities are approximated by polynomial ansatz functions parameterized by the unknown nodal displacements $\theta(t)$ and nodal electric potentials $\phi(t)$.

The obtained coupled structural dynamics applying the piezoelectric constitutive law of the piezoelectric structure can be formulated as

$$\begin{bmatrix} M_{\mathrm{ss}} & 0 \\ 0 & 0 \end{bmatrix} \begin{bmatrix} \ddot{\theta}(t) \\ \ddot{\phi}(t) \end{bmatrix} + \begin{bmatrix} K_{\mathrm{ss}} & K_{\mathrm{s}\phi} \\ K_{\mathrm{s}\phi}^{\mathrm{T}} & K_{\phi\phi} \end{bmatrix} \begin{bmatrix} \theta(t) \\ \phi(t) \end{bmatrix} = \begin{bmatrix} f(t) \\ q(t) \end{bmatrix}. \quad (1)$$

Hereby, the right hand side is given by the external forces f and the external electric charge q. The mass and stiffness matrices of the structure are M_{ss} and K_{ss}, whereas the matrix $K_{\mathrm{s}\phi}$ couples the electric field and structural displacements in the piezoelectric material.

2.1 Piezoelectric actuation as system inputs

Electrical voltages are applied across potential electrodes and a common grounded electrode for actuation. To incorporate these system inputs into the model, the vector of the electrical potential degrees of freedom (DOFs) ϕ is partitioned into potentials of the potential electrodes ϕ_{p}, grounded electrodes ϕ_{g} and interior nodes ϕ_{i}. Then, the structural dynamics can be written as (Becker et al. (2006))

$$\begin{bmatrix} M_{\mathrm{ss}} & 0 & 0 & 0 \\ 0 & 0 & 0 & 0 \\ 0 & 0 & 0 & 0 \\ 0 & 0 & 0 & 0 \end{bmatrix} \begin{bmatrix} \ddot{\theta} \\ \ddot{\phi}_{\mathrm{i}} \\ \ddot{\phi}_{\mathrm{p}} \\ \ddot{\phi}_{\mathrm{g}} \end{bmatrix} + \begin{bmatrix} K_{\mathrm{ss}} & K_{\mathrm{si}} & K_{\mathrm{sp}} & K_{\mathrm{sg}} \\ K_{\mathrm{si}}^T & K_{\mathrm{ii}} & K_{\mathrm{ip}} & K_{\mathrm{ig}} \\ K_{\mathrm{sp}}^T & K_{\mathrm{ip}}^T & K_{\mathrm{pp}} & K_{\mathrm{pg}} \\ K_{\mathrm{sg}}^T & K_{ig}^T & K_{\mathrm{pg}}^T & K_{\mathrm{gg}} \end{bmatrix} \begin{bmatrix} \theta \\ \phi_{\mathrm{i}} \\ \phi_{\mathrm{p}} \\ \phi_{\mathrm{g}} \end{bmatrix} = \begin{bmatrix} f \\ q_{\mathrm{i}} \\ q_{\mathrm{p}} \\ q_{\mathrm{g}} \end{bmatrix}.$$

Now the grounded potential DOFs are set to zero, $\phi_{\mathrm{g}} = 0$, and the inner potential degrees of freedom (DOFs) ϕ_{i} are eliminated, which yields

$$\begin{bmatrix} M_{\mathrm{ss}} & 0 \\ 0 & 0 \end{bmatrix} \begin{bmatrix} \ddot{\theta} \\ \ddot{\phi} \end{bmatrix} + \begin{bmatrix} H_{\mathrm{ss}} & H_{\mathrm{s}\phi} \\ H_{\mathrm{s}\phi}^{\mathrm{T}} & H_{\phi\phi} \end{bmatrix} \begin{bmatrix} \theta \\ \phi_{\mathrm{p}} \end{bmatrix} = \begin{bmatrix} f \\ q_{\mathrm{p}} \end{bmatrix}, \quad (2)$$

with the following submatrices

$$H_{\mathrm{ss}} = K_{\mathrm{ss}} - K_{si} K_{\mathrm{ii}}^{-1} K_{\mathrm{si}}^T \quad (3)$$
$$H_{\mathrm{sp}} = K_{\mathrm{sp}} - K_{si} K_{\mathrm{ii}}^{-1} K_{\mathrm{ip}} \quad (4)$$
$$H_{\mathrm{pp}} = K_{\mathrm{pp}} - K_{ip}^T K_{\mathrm{ii}}^{-1} K_{\mathrm{ip}}. \quad (5)$$

The piezoelectric tube possess metal electrodes at its surface, on which the equal electrical potential condition must hold, i.e. all nodal electrical potentials are identical.

Finally, if the patch is driven as an actuator, it directly follows

$$M_{\mathrm{ss}} \ddot{\theta} + H_{\mathrm{ss}} \theta = -H_{\mathrm{sp}} \phi_{\mathrm{e}} + f \quad (6)$$

where one (scalar) potential ϕ_{e} for each actuator patch remains. The external forces f denote disturbances of the controlled system that are unknown to the control and therefore omitted in the following control design. For the investigated twin–electrode configuration and two–dimensional lateral scan motion, the input voltages applied to two opposite patch electrodes with different signs are combined to one system input according to Fig. 1, which gives a system with two inputs

$$M\, \ddot{\theta}(t) + K\, \theta(t) = \beta u(t), \quad (7)$$

with symmetric mass and stiffness matrices $M = M_{\mathrm{ss}}, K = H_{\mathrm{ss}}$ and the input matrix $\beta = -H_{\mathrm{sp}}$.

The two physical controlled output variables $w(t)$ are given by the output matrix Γ as a linear combination of the nodal displacements,

$$w(t) = \Gamma \theta(t). \quad (8)$$

2.2 Modal transformation and modal truncation

For modal transformation, the transformation $\theta(t) = \Phi\, x(t)$ is applied to the system in physical coordinates. The columns of the transformation matrix Φ are given by the eigenvectors φ_k obtained from the solution of the generalized eigenvalue problem

$$\left(K - \omega^2 M\right)\, \varphi = 0. \quad (9)$$

Exemplarily, the mode shape of the first eigenvector φ_1 is shown in Fig. 1. Left–multiplication of (7) with Φ^{T} yields a decoupled set of differential equations

$$\ddot{x}(t) + \Omega x(t) = b\, u(t) \quad (10)$$

with the spectral matrix $\Omega = \mathrm{diag}\left[\omega_1^2, \omega_2^2, \ldots, \omega_N^2\right]$ and the transformed input vector $b = \Phi^{\mathrm{T}} \beta = [b_1, b_2, \ldots, b_N]^{\mathrm{T}}$. By restricting the transformation matrix Φ to the first $m \ll N$ low–frequency eigenvectors, the system order can be efficiently reduced. The necessary number $m \ll N$ of retained modes depends on the considered structure and the frequency bandwidth of the input $u(t)$ required to realize a desired transition. If highly dynamic motion is desired, m has to be chosen larger in order to accurately approximate the system behavior. For the piezotube, a residual mode or a feedthrough-term, which is frequently used to compensate the unmodeled dynamics of the truncated modes, shows no significant contribution to the position of the zeros in the reduced system for $m \geq 3$ retained modes and is thus neglected.

Finally, the controlled variable defined by (8) is given with respect to the modal states by $w(t) = Cx(t)$, where $C = \Gamma\Phi$ denotes the transformed output vector.

3. FEEDFORWARD CONTROL DESIGN

The feedforward control design is conducted for each scan direction separately exploiting that the dynamics of the x– and y– direction can be assumed to be completely decoupled as verified in Fig. 4. For that purpose, subsystems are built describing the input/output–dynamics of the x or y-direction. The obtained systems then read

$$\ddot{x}_k + \omega_k^2 x_k = b_k u_1, \quad w_1 = \sum_{k=1}^{m} c_k x_k \tag{11}$$

for each scan direction $1 \in \{x, y\}$. Note that due to the rotational symmetry, the bending modes obtained from the FE discretization can always be rotated such that they are solely excited by the input voltage of one scan direction.

A flatness–based inversion procedure as outlined in Fig. 2 is proposed that uses input and state parameterizations in terms of a so–called flat output as a parameterizing variable to derive a control command $u_l(t)$ that makes the piezoscanner tip follow a desired rest–to–rest motion between given initial and final stationary values w_0^* and w_T^*. The proposed model-based approach offers fast computation of the control command, because no iterative solution is necessary. Furthermore, input shaping techniques possess minimum transition times of half of the period of the lowest mode and yield step inputs which are not well suited for amplifiers and any additional feedback control. It has been shown in simulations that the minimal transition time for the flatness–based approach is only limited by the wave propagation time between system input and output. Thus, both of these limitations of other feedforward control techniques are overcome by the proposed approach.

3.1 Flatness–based inversion procedure

Roughly speaking, the notion of differential flatness states that any system state and system input can be expressed in terms of a parameterizing flat output and its time–derivatives up to certain order (see Fliess et al. (1995) for the notion of differential flatness and Rudolph and Woittennek (2002); Becker et al. (2006a) and references herein for use of this notion for control of flexible structures). Starting from the modal representations (11), it can be shown that the modal representation is flat with respect to a flat output $y(t)$, given by

$$y(t) = \sum_{k=1}^{m} \frac{\omega_k^2}{b_k \prod_{j=1, j\neq k}^{m} \left(1 - \frac{\omega_k^2}{\omega_j^2}\right)} x_k(t).$$

This variable and its derivatives parameterize the modal states $x_k(t)$, $k \geq 1$ and the system input $v(t)$ according to,

$$x_k(t) = \frac{b_k}{\omega_k^2} D_x^k(s)\{y(t)\}\Big|_{s^j = \frac{d^j}{dt^j},\ j \in \ _0} \tag{12}$$

$$\text{with} \quad D_x^k(s) = \prod_{j=1, j\neq k}^{N} \left(1 + \frac{s^2}{\omega_j^2}\right),$$

$$u(t) = D_u(s)\{y(t)\}\Big|_{s^j = \frac{d^j}{dt^j},\ j \in \ _0} \tag{13}$$

$$\text{with} \quad D_u(s) = \prod_{j=1}^{m} \left(1 + \frac{s^2}{\omega_j^2}\right).$$

Hereby the operator s denotes differentiation in the time domain and m is the subsystem order of the previous section. Singularities of (12) and (13) are avoided because non–controllable and non–observable modes are not incorporated in the subsystem models.

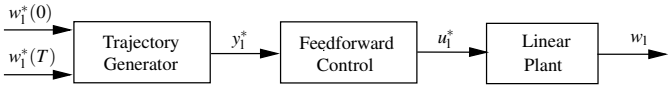

Fig. 2. Flatness-based feedforward control design procedure for one subsystem describing the dynamics of the direction $1 \in \{x, y\}$ (the asterisk denotes desired trajectories).

It is important to note that in general the flat output obeys no direct physical interpretation but serves only as a calculation variable in the feedforward control design procedure outlined in Fig. 2. If the considered flexible structures are analytically modelled and thus described by partial differential equations, the parameterizations become infinite series (Becker and Meurer (2007)).

3.2 Motion planning

For evaluation of the derived parameterizations (12) and (13), an appropriate trajectory $y^*(t)$ must be planned for the flat output that realizes the transition between stationary initial and final values y_0^* and y_T^*,

$$y^*(t) = y_0^* + (y_T^* - y_0^*)\Psi_{\sigma,T}(t), \quad \Psi_{\sigma,T}(t) \in [0,1], \tag{14}$$

where the initial and final values y_0^* and y_T^* are determined from the static solution of (10) and the desired (physical output) stationary values w_0^* and w_T^* . The trajectory (14) is inserted into (13) to obtain the feedforward control $u^*(t)$ that makes the physical output $w(t)$ follow the smooth trajectory $w^*(t)$ from the initial to the desired final values, $w_1^*(0)$ and $w_1^*(T)$ within the transition time–interval $t \in [0, T]$.

Obviously, the convergence of these series is guaranteed if the modal representation is of finite dimension as in (10). For infinite–dimensional systems however, convergence is a necessary condition in order to perform truncation of the series (12), (13). This in turn implies that the trajectories must be smooth functions. Additionally, its time derivatives must be zero for $t < 0$ and $t > T$ in order to realize the desired transition between stationary states, which results in non–analytic functions at the two points $t = \{0, T\}$, see Becker and Meurer (2007) for details on convergence analysis.

As an advantage of this design approach, the control input and state trajectories can be iteratively replanned in order to meet certain control performance criteria, e.g. actuator saturation.

3.3 Realization of the scan trajectory

The trajectory of the rectangular raster scan motion in the xy–plane consists of a staircase x–displacement and a triangular y–displacement. This scan pattern poses additional challenge to the trajectory tracking compared to the motion conventionally investigated, where the displacement normal to the triangular portion is generated by a slowly increasing ramp voltage of constant slope (Abramovitch et al. (2007)). Following the approach of Perez et al. (2004), the scan trajectory is divided into two parts: the transition section and the tracking section with active scan time T_a. For the scan trajectory, rest–to–rest motion is desired in x-direction. The input parameters to the trajectory generator in Fig. 3 are the initial displacement $w_x^*(0)$ and the final displacement $w_x^*(T)$ after the step.

In the fast scanning direction, constant velocity is needed during the scan process with velocity reversals for every new x-coordinate. Exploiting the system linearity, the triangular scan

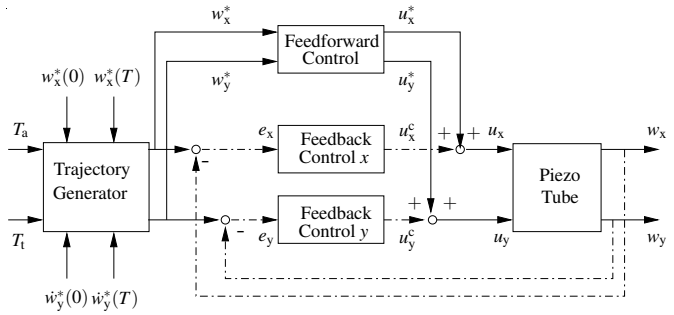

Fig. 3. Block diagram of the feedforward control scheme (solid lines) and the feedback control scheme (dashed–dotted lines) for two–degree–of–freedom tracking control.

motion is generated by prescribing a smooth step as velocity output trajectory $\dot{w}^*(t)$ instead of a displacement $w^*(t)$ by (14). Consequently, the parameterization (13) yields the input signal derivative $\dot{v}(t)$, which is integrated once to obtain the desired input voltage for the fast scanning direction y. Hence, the inputs to the system generator are the desired initial and final velocities $\dot{w}_y^*(0)$ and $\dot{w}_y^*(T)$.

4. SIMULATION OF TRAJECTORY TRACKING

The FE model of the piezoelectric tube scanner is based on the twin–electrode excitation mode in Fig. 1. The control loop with feedforward and feedback components is illustrated in Fig. 3.
To account for realistic uncertainties of the piezotube, a test model is built, in which the weight of the sample mass attached to the tip is varied to achieve a change of the eigenfrequencies in the order of 1%–2% compared to the nominal model, and a tube eccentricity of 30 μm in x-and y-direction is introduced to amplify the coupling between x– and y–motion. For this test model, the robustness of the trajectory tracking is enhanced by means of the two–degree–of–freedom design, where the feedback loop with the dashed–dotted lines in Fig. 3 is added to the feedforward control scheme. The obtained displacements w_x and w_y are compared with the desired trajectories w_x^* and w_y^*. The tracking errors e_x and e_y are fed into two SISO controllers. The electrode input voltages are then composed of the controller portion u_x^c and the feedback portion u_x^* for x–displacement, and of u_y^c and u_y^* for y–motion, respectively.

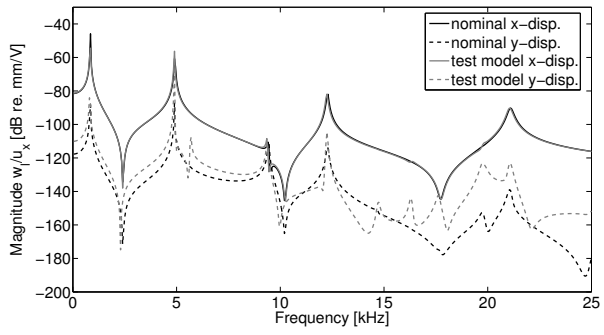

Fig. 4. x-displacement and y-displacement frequency response of the piezoelectric tube for x-electrode excitation.

4.1 Nominal and test model

The magnitudes of the frequency response functions from the x–electrode driving voltage $+u_x$ to the displacement outputs w_x and w_y are shown in Fig. 4 for the nominal model of the tube assembly and the test model. The coupling between x–axis excitation and y–axis motion is weak in the nominal case, illustrated by the approximately 40 dB lower amplitude of w_y in comparison to w_x. This observation justifies the disregard of coupling effects in the feedforward design and the implementation of SISO controllers for the MIMO system in the two–degree–of–freedom approach. The x-displacement response of the test model is almost identical to the nominal case, while tube eccentricity increases the coupling to the y-displacement by approximately 10 dB in the low–frequency limit. Furthermore, Fig. 4 demonstrates that the displacement responses are dominated by a resonance at 850 Hz. Due to the tube symmetry, the displacement responses from y–electrode excitation are identical to the x–electrode excitation and need not to be shown.

4.2 Feedforward control of the nominal model

In the following simulations, the scan frequency is set to 250 Hz for the triangular trajectory in y-direction, which is typically referred to as the fast scanning direction. This value corresponds to more than 1/4th of the first resonance frequency. Note that the scanning frequency is typically limited to approximately 1/100th of the first resonance frequency to avoid the excitation of structural vibrations (Aphale et al. (2007)). Steps along the x-direction are performed every 2 ms at each reversal point of the triangular trajectory.
The feedforward control is calculated according to Sec. 3 for a subsystem order $m = 3$ for which convergent behavior of the series has been proven, i.e. increasing the order m does not change the obtained feedforward control. Fig. 5 shows u_x^* and u_y^*, and the uncompensated voltages u_x^u and u_y^u obtained from the desired displacement trajectories w_x^* and w_y^* by division with the

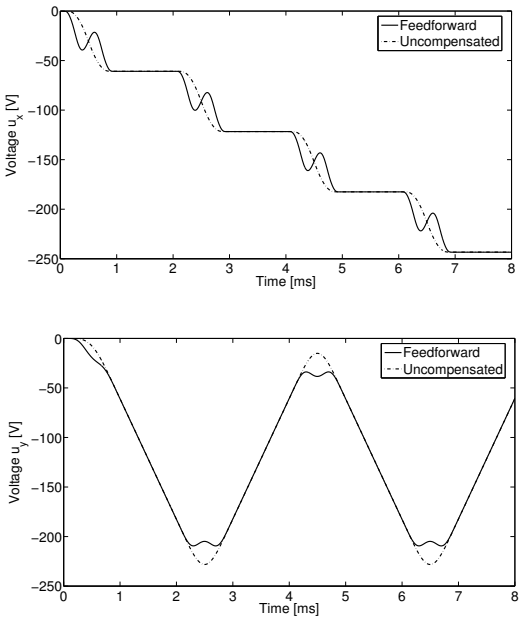

Fig. 5. Input voltages of potential electrodes (top: x–electrode; bottom: y–electrode).

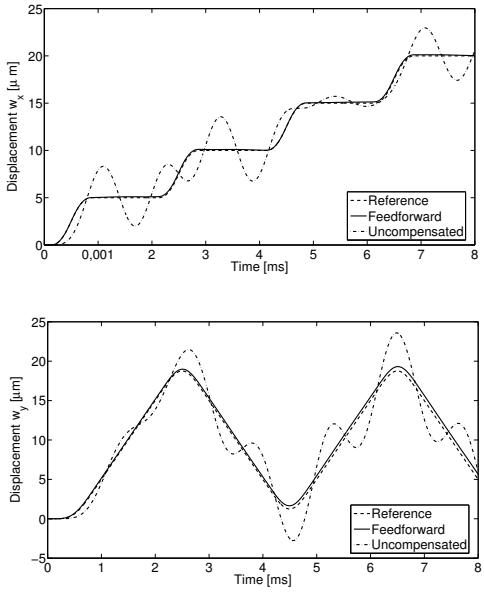

Fig. 6. Feedforward control of the nominal piezotube model (top: x–displacement; bottom: y–displacement).

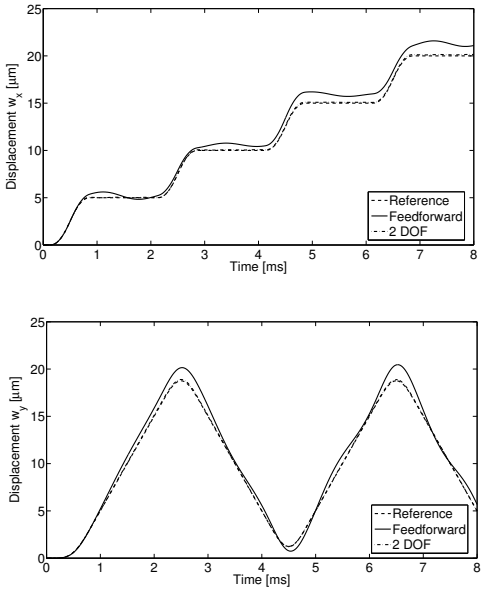

Fig. 7. Two–degree–of–freedom control of the test model(top: x–displacement; bottom: y–displacement).

static gain of the transfer function from x–electrode excitation to x–displacement of Fig. 4. It can be seen that minimization of the resonances of the tube scanner is achieved in the feedforward scheme by modifying the shape of the input voltages during the transition time. To this end, oscillatory components are added to the driving signals to compensate the structural vibrations. Both signals, the uncompensated and the feedforward driving voltages, are well below the limit of piezoelectric voltage saturation. Especially, the amplitude of the feedforward voltage is in the same order as the uncompensated one, meaning that feedforward control does not negatively affect the scan range of the piezotube.

In the simulations, the uncompensated input voltages and the feedforward control commands are applied to the nominal piezoelectric tube scanner system, i.e. the model parameters for the control design and in the simulation model are identical. The obtained displacements w_x and w_y are shown in Fig. 6 in comparison with the reference trajectories. In the uncompensated case, the output displacements strongly deviate from the desired trajectory due to the excitation of structural vibrations in the piezotube. The oscillation is dominated by the first resonance of the piezoscanner. In contrast, the output displacements almost perfectly track the reference trajectory for the feedforward control. The small deviations observed in the feedforward scheme are due to the neglected cross–coupling terms in the generation of the input voltages u_x^* and u_y^*. The feedforward scheme thus enables fast and accurate scanning for the nominal model.

4.3 Two–degree–of–freedom control of the test model

In the context of trajectory tracking in atomic force microscopy applications, two–degree–of–freedom control was applied to piezoelectric actuators by Leang and Devasia (2002) to separately treat the suppression of hysteresis and creep by feedback control, and the compensation of induced vibrations by feedforward control. Schitter et al. (2003) used a two–degree–of–freedom control approach to increase the scan speed of piezoelectric tube scanners in z–direction.

In the present approach, the feedback loop is designed to achieve robust trajectory tracking in the xy–plane. Two identical SISO PI controllers are designed for the x– and y–motion dynamics. They feed back the corresponding displacement signals as depicted in Fig. 3 and possess a bandwith above the first resonance frequency of the scanner assembly.

Fig. 7 demonstrates the improvement in scan accuracy for the two–degree–of–freedom control scheme in comparison to the feedforward approach in the simulation of the test model. Due to the variation of the eigenfrequencies, the responses obtained from the modal-based feedforward controller of Sec. 3.1 significantly deviate from the prescribed reference trajectories, oscillatory components are visible in Fig. 7(a) and Fig. 7(b). Furthermore, the stronger coupling of x and y-dynamics lead to a linearly increasing steady–state error as observed in Fig. 7(a) as the deviation between the reference step trajectory and the feedforward step response. On the other hand, the feedback loop in the two–degree–of–freedom design compensates for the feedforward tracking error such that accurate scanning is always achieved. It is thus robust against variations in the eigenfrequencies of the tube scanner assembly as well as increased coupling between the x– and y– directions.

Simultaneously, the control effort u_x^c and u_y^c remains low since the main contribution to the electrode driving voltages u_x and u_y is still supplied from the feedforward portions u_x^* and u_x^* as illustrated in Fig. 8. The compensation of the dynamics–coupling errors is observed as a slight triangular shape in the feedback component u_y^c of the y–electrode driving voltage and accordingly small steps in u_x^c.

The raster scan trajectories in the xy-plane are shown in Fig. 9 obtained by the simulations with the piezotube test model with eccentrity and changed tip mass. The strong deviations in the feedforward–control raster scan are apparent. It is furthermore observed that the optimal scan trajectory approaches a circular shape during the transition time, resulting in a simultaneous smooth transfer at the reversal points of the triangular motion and the steps of the staircase displacement. Again, the two–degree–of–freedom design tracks the reference trajectory with high accuracy.

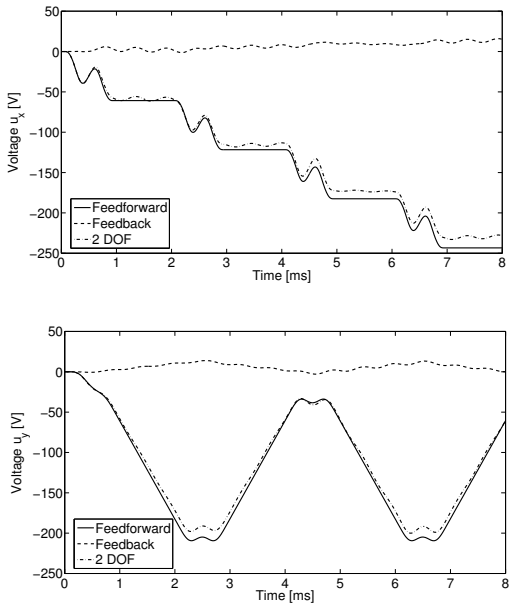

Fig. 8. Comparison of the feedforward and feedback components of the electrode driving voltages in two–degree–of–freedom control (top: *x*–electrode; bottom: *y*–electrode).

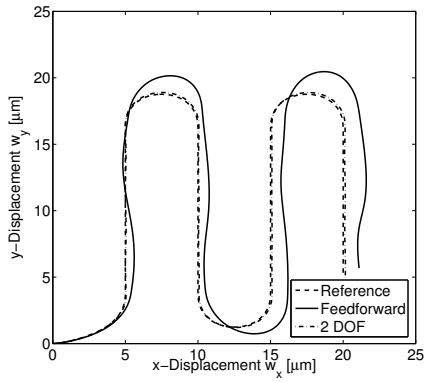

Fig. 9. Two-dimensional raster scan trajectory.

5. CONCLUSIONS

A two–degree–of–freedom control scheme is proposed for the tracking of prescribed scan trajectories in the lateral *xy*–plane with piezoelectric tube scanners, that are used in atomic force microscopy for relative positioning of the sample and the probe. A FE model of the tube scanner is used to determine the driving voltages of the potential electrodes by means of a flatness–based feedforward control scheme. Simulation results demonstrate the high accuracy of the obtained feedforward control. In two–degree–of–freedom control, SISO PI-controllers are designed to ensure robustness in closed–loop operation by means of displacement feedback to achieve exact asymptotic tracking under uncertainties that may be introduced by tube eccentricity and variations of the sample mass. Simulations with a modified model that significantly deviates from the nominal design model verify the good tracking performance of the proposed control approach.

Currently, the use of induced voltages at sensor electrodes in single–electrode excitation mode as feedback signals to avoid the need for additional displacement sensors in closed–loop operation of piezoelectric tubes is under investigation. Furthermore, the control of three–dimensional scanning applications is analyzed, focusing on the compensation of the coupling from the lateral scan motion into the normal *z*–direction which is significantly stronger in single–electrode excitation compared to twin electrode excitation.

REFERENCES

D.Y. Abramovitch, S.B. Andersson, L.Y. Pao, and G. Schitter. A tutorial on the mechanisms, dynamics, and control of atomic force microscopes. In *Proceedings of the American Control Conference*, New York, NY, USA, pages 3488–3502, 2007.

S. Aphale, A.J. Fleming, and S.O.R. Moheimani. High speed nano-scale positioning using a piezoelectric tube actuator with active shunt control. *Micro & Nano Letters*, volume 2, pages 9–12, 2007.

J. Becker, O. Fein, M. Maess, and L. Gaul. Finite element-based analysis of shunted piezoelectric structures for vibration damping. *Computers & Structures*, volume 84, pages 2340–2350, 2006.

J. Becker, T. Meurer, and L. Gaul. Flatness-Based Feedforward Control Design for Flexible Structures. In *Proceedings of the IEEE International Conference on Control Applications*, Munich, Germany, pages 650–655, 2006.

J. Becker and T. Meurer. Feedforward tracking control for non–uniform timoshenko beam models: combining differential flatness, modal analysis and FEM. *ZAMM*, volume 87 pages 37–58, 2007.

G. Binning and D.P.E. Smith. Single-tube three-dimensional scanner for scanning tunneling microscopy. *Review of Scientific Instruments*, volume 57, pages 1688–1689, 1986.

R.G. Carr. Finite element analysis of PZT tube scanner motion for scanning tunnelling microscopy. *Journal of Microscopy*, volume 152, pages 379–385, 1988.

O.M. El Rifai and K. Youcef-Toumi. Coupling in piezoelectric tube scanners used in scanning probe microscopes. In *Proceedings of the American Control Conference*, Arlington, VA, USA, pages 3251–3257, 2001.

A. J. Fleming and S.O.R. Moheimani. Sensorless vibration suppression and scan compensation for piezoelectric tube nanopositioners. *IEEE Transactions on Control Systems Technology*, volume 14, pages 33–44, 2006.

M. Fliess, J. Lévine, P. Martin, and P. Rouchon. Flatness and defect of non–linear systems: introductory theory and examples. *International Journal of Control*, volume 61, pages 1327–1361, 1995.

K.K. Leang and S. Devasia. Hysteresis, creep, and vibration compensation for piezoactuators: feedback and feedforward control. In *Proceedings of the 2nd IFAC Conference on Mechatronic Systems*, Berkeley, CA, USA, pages 283–289, 2002.

Y. Li and J. Bechhoefer. Feedforward control of a closed-loop piezoelectric translation stage for atomic force microscope. *Review of Scientific Instruments*, volume 78, pages 013702 (1–8), 2007.

J. Maess, A.J. Fleming, and F. Allgöwer. Simulation of piezoelectric tube actuators by reduced finite element models for controller design. In *Proceedings of the American Control Conference*, New York, NY, USA, pages 4221–4226, 2007.

H. Perez, Q. Zou, and S. Devasia. Design and control of optimal scan trajectories: scanning tunneling microscope example. *Journal of Dynamic Systems, Measurement and Control*, volume 126, pages 187–197, 2004.

J. Rudolph and F. Woittennek. Flatness based boundary control of piezoelectric benders. *at–Automatisierungstechnik*, volume 50, pages 412–421, 2002.

G. Schitter, A. Stemmer, and F. Allgöwer. Robust 2DOF-control of a piezoelectric tube scanner for high speed atomic force microscopy. In *Proceedings of the American Control Conference*, Denver, CO, USA, pages 3720–3725, 2003.

G. Schitter, F. Allgöwer, and A. Stemmer. A new control strategy for high-speed atomic force microscopy. *Nanotechnology*, volume 15, pages 108–114, 2004.

Q. Sun and R.A. Wolkow. Three-dimensional displacement analysis of a piezoelectric tube scanner through finite element analysis of a tube assembly. *Review of Scientific Instruments*, volume 77, pages 113701 (1–9), 2006.

S. Tien, Q. Zou, and S. Devasia. Iterative control of dynamics-coupling-caused errors in piezoscanners during high-speed AFM operation. *IEEE Transactions of Control System Technology*, volume 13, pages 921–931, 2005.